Covalent and noncovalent functionalization of pristine and defective graphene by cyclohexane and dehydrogenated derivatives

Ceren Sibel Sayin [a], Daniele Toffoli [b,*], Hande Ustunel [a,*]

[a] Department of Physics, Middle East Technical University, Dumlupinar Bulvari 1, 06800 Ankara, Turkey
[b] Dipartimento di Scienze Chimiche e Farmaceutiche, Università degli Studi di Trieste, Via L. Giorgieri 1, I-34127 Trieste, Italy

ARTICLE INFO

Accepted 19 May 2015

Keywords:
Graphene
Cyclohexane
Cyclohexene
Cyclohexyl
Functionalization
Density functional theory

ABSTRACT

The interaction of cyclohexane (C_6H_{12}), cyclohexyl ($C_6H_{11}^*$) and cyclohexene (C_6H_{10}) with both pristine and defective graphene (single vacancy and a carbon adatom), is systematically investigated within the density functional theory framework. C_6H_{12} physisorbs on both pristine and defective graphene while C_6H_{10} chemisorbs on graphene in the presence of an adatom. The $C_6H_{11}^*$ radical binds covalently with the graphene substrate in all adsorption geometries considered.

1. Introduction

Advances in the fabrication and processing of graphene [1] has greatly expanded its potential applications in the last decade. In a short span of time, graphene has gone from being a novel source of fascinating physical phenomena [2,3] to having sophisticated applications in various fields including optics, catalysis and device technology [4–7]. Owing to its unique, defect-free sp^2 network structure, graphene possesses unusually high carrier mobility [8], thermal conductivity [9], and mechanical strength [10]. The distinguishing feature of its band structure is the occurrence of double cones centered at the six Fermi points in the hexagonal Brillouin zone, referred to as Dirac cones. Contributed by the delocalized π and π^* orbitals, the apices of the Dirac cones touch at a single point resulting in a linear electronic dispersion and a zero density of states at the Fermi level.

Chemical functionalization of graphene is a versatile technique with various applications in band gap engineering, gas sensing, and spintronics [11–15]. The species range from single atoms [16,17], all the way to large polymers [18]. Functionalization may be achieved via covalent or noncovalent bonding [19]. Covalent bonding is usually accompanied by the destruction of the linear dispersion and the opening of a band gap at the Fermi points. Noncovalent functionalization, on the other hand, relies on weak dispersive forces and often leaves the band structure unchanged. A charge transfer may nonetheless occur even for noncovalent bonding. In the study by Coletti et al. [20] the Fermi level of a graphene sheet, n-doped by the SiC substrate, was restored to its original location at the Dirac point by gradually increasing the surface coverage of tetrafluoro-tetracyanoquinodimethane (F4-TCNQ) molecules.

Defects and impurities can be introduced in the network to facilitate functionalization [13,21,22]. Point defects, such as single or double vacancies and adatoms locally alter the electronic structure and act as functionalization centers [23,24]. Due to their high formation energies, such defects are present with negligible concentration in graphene produced through standard sample growth processes. However, controlled defect creation is possible via methods such as particle irradiation and chemical treatment [25].

Cyclohexane (C_6H_{12}) is a monocyclic hydrocarbon, synthesized from hydrogenation of benzene and produced on large industrial scales primarily for use in the production of adipic acid, a nylon intermediate [26]. Interaction between C_6H_{12} (and its dehydrogenated or oxygenated derivatives) and graphene-based materials has been sporadically explored in the literature. In an experimental study by Yu *et al.* [27], N-doped carbon nanotubes (CNTs) were

* Corresponding authors.
E-mail addresses: toffoli@units.it (D. Toffoli), ustunel@metu.edu.tr (H. Ustunel).

shown to display catalytic activity towards the aerobic oxidation of cyclohexane. Bittner et al. [28] and Díaz et al. [29] investigated the adsorption of non-cyclic and cyclic molecules on carbon nanotubes (CNT), including C_6H_{12} and C_6H_{10}. In a density functional theory (DFT) study by Zhao et al. [30], the adsorption of C_6H_6, C_6H_{12} and 2,3-dichloro-5,6-dicyano-1,4-benzoquinone (DDQ) on a single-walled CNT were explored. C_6H_{12} was found to bind slightly more strongly than benzene even though all molecule–CNT interactions were of dispersive nature. DFT was also applied by Yang et al. [31] to study the mechanism of CNT-catalyzed oxidation of C_6H_{12} by molecular oxygen.

In this work, we explore the interaction of cyclohexane (C_6H_{12}), the cyclohexyl radical ($C_6H_{11}^*$) and cyclohexene (C_6H_{10}) with both pristine and defective graphene using DFT. The graphene defects under investigation are a single vacancy and a C adatom. While in C_6H_{12}, carbon atoms are sp^3-hybridized, C_6H_{10} is characterized by a single C—C double bond. $C_6H_{11}^*$, on the other hand, is a radical with high reactivity. The aim of this study is to investigate how, and to which extent, local changes in the electronic structure of the adsorbate affect the graphene-molecule and defect-molecule interaction.

2. Computational details

The calculations were performed using plane wave-based density functional theory as implemented in the Quantum Espresso code suite [32]. Vanderbilt ultrasoft pseudopotentials [33] within GGA(PBE [34]) were used to describe the ion-electron interaction. Van der Waals dispersion forces were included to treat the molecule-graphene interaction for physisorbed species. For spin-unpolarized configurations, a van der Waals correction to the exchange-correlation functional was included in a fully self-consistent scheme through the Soler algorithm [35]. In particular, a vdW-DF2 type van der Waals functional was used with the C09 exchange (vdW-DF2^{C09x}) [36,37] along with a kinetic energy cutoff of 30 Ryd. Due to the lack of a spin-polarized implementation for self-consistent van der Waals functionals, the PBE-D2 method of Grimme [38] was used for those cases where spin polarization is important. Covalently bonded species instead were handled using conventional GGA. Marzari–Vanderbilt cold smearing with a broadening of 0.02 Ryd was adopted for Brillouin zone integration [39] with Monkhorst-Pack meshes of $6\times6\times1$ and $3\times3\times1$ respectively for the 3×3 and 6×6 simulation cells used in our calculations. A separation between periodic images of at least 12 Å was allowed in all calculations. Using these parameters, the lattice constant of graphene was calculated to be 2.46 Å at the GGA, vdW-DF2^{C09x} and PBE-D2 levels of theory, in agreement with previously reported values [40]. Geometry optimization was performed with the Broyden–Fletcher–Goldfarb–Shanno (BFGS) algorithm with a force convergence threshold of 0.025 eV/Å per atom. Figures were generated using the open source visualization program XCrySDen [41]. The geometry optimization for isolated molecules was carried out in a large cubic unit cell at the Γ point. The optimized geometries are shown in Fig. 1 and calculated structural parameters agree well with values reported in the literature [42,43].

In order to understand coverage effects, molecular adsorption on pristine graphene was explored using coverages $\Theta = 1/36$ and $\Theta = 1/9$ monolayer (ML), which correspond to surface densities of one molecule per 6×6 and 3×3 simulation cells respectively. In the terminology adopted in this study, coverage refers to the number of molecules per primitive unit cell. The 1/36 ML coverage corresponds to a center-to-center intermolecular distance of about 14.7 Å, while $\Theta = 1/9$ ML corresponds to full coverage for flat geometries. Fig. 2 illustrates a representative flat adsorption geometry for C_6H_{12} for the two coverages.

Calculations involving defective graphene were performed only in the 6×6 supercell. The defect formation energies are calculated from:

$$E_f = E_{def-gr} - n\mu_C - E_{gr}, \tag{1}$$

where E_{gr} is the total energy of the pristine graphene sheet, E_{def-gr} is the total energy of defective graphene and $\mu_C = E_{gr}/N$ is the chemical potential of carbon. Here N is the number of C atoms in the simulation cell, $n = -1$ for the vacancy and $n = +1$ for an adatom. The GGA formation energies for the single vacancy and the adatom are calculated to be 7.56 eV and 6.41 eV respectively, both in good agreement with previous results [44,45].

The molecular adsorption energies are calculated using:

$$E_{ads} = E_{gr} + E_{mol} - E_{mol+gr} \tag{2}$$

where E_{mol+gr} is the total energy of the combined system, E_{gr} is the energy of the pristine or defective graphene sheet and E_{mol} is the energy of an isolated neutral C_6H_{12}, $C_6H_{11}^*$ or C_6H_{10} molecule, all calculated with the same computational parameters. With this definition, positive adsorption energies correspond to stable adsorption geometries. For physisorbed species, E_{mol} and E_{gr} were both calculated using the relevant vdW-based exchange-correlation functionals while for chemisorption, traditional GGA was used. Spin polarization was employed as needed.

Charge density differences for chemisorbed species were calculated by using the formula:

$$\Delta\rho(\vec{r}) = \rho_{mol+gr}(\vec{r}) - \rho_{gr}(\vec{r}) - \rho_{mol}(\vec{r}) \tag{3}$$

where $\rho_{mol+gr}(\vec{r})$ is the electronic charge density of the pristine or defective graphene substrate interacting with the adsorbate, $\rho_{gr}(\vec{r})$ is the charge density of either pristine or defective graphene alone and $\rho_{mol}(\vec{r})$ is the charge density of the isolated molecule.

Charge transfer between the graphene network and the adsorbates upon adsorption was investigated using the Bader charge analysis as implemented by the Henkelman group [46]. The charge on $C_6H_{11}^*$ due to adsorption was determined taking as reference the neutral C_6H_{11} radical.

3. Results and discussion

3.1. Electronic properties of pristine and defective graphene

As a basis for our discussion on molecular adsorption, we briefly review the electronic properties of pristine graphene and graphene with point defects. Fig. 3 displays the band structures of pristine graphene as well as graphene with a single vacancy and a C adatom calculated using the GGA exchange-correlation potential. Due to zone folding, the Fermi level now appears at the Γ point. In the case of the single vacancy, spin polarization lifts the degeneracies while the Fermi level is depressed below the original location. The adatom introduces a flat state lying along the Fermi level throughout the Brillouin zone while degeneracies around the Fermi level are lifted. For the single vacancy, spin-unpolarized GGA and vdW-DF2^{C09x} calculations both yield a ground state where one of the three atoms surrounding the vacancy undergoes an out-of-plane displacement of about 0.6 Å. The remaining two atoms approach each other to a distance of 2.0 Å. Spin polarized GGA and PBE-D2 calculations, on the other hand, both converge to a flat geometry with a magnetization of about 1.40 μ_B per simulation cell. The GGA spin-polarized ground state is energetically more favorable by 0.19 eV per vacancy with respect to the GGA spin zero state, in good agreement with past investigations [47–49].

The most stable geometry for the carbon adatom is the bridge position where the adatom resides on top of the mid-point of a C—C

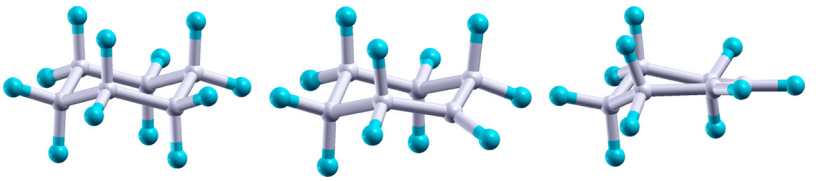

Fig. 1. Optimized structures of isolated C_6H_{12}, $C_6H^*_{11}$ and C_6H_{10} molecules.

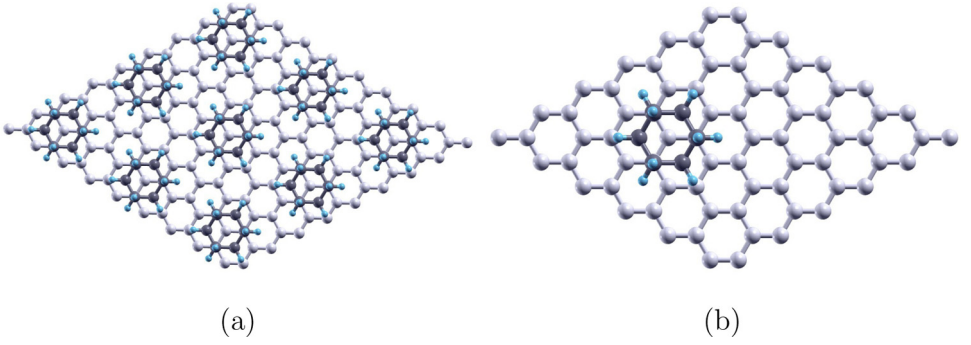

Fig. 2. Flat C_6H_{12} adsorption on pristine graphene with $\Theta = 1/9$ (a) and $\Theta = 1/36$ (b) coverages.

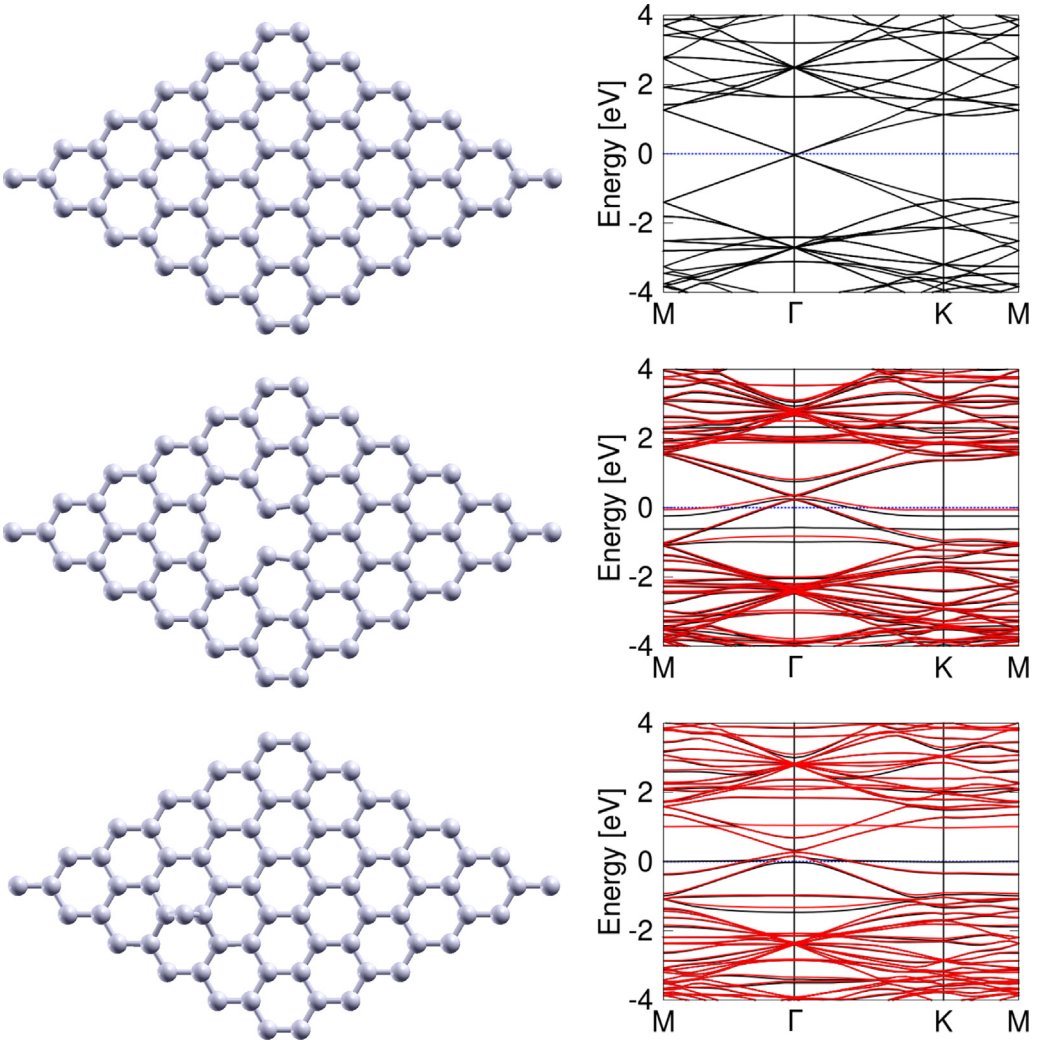

Fig. 3. Optimized geometries and band structures of pristine graphene, and defective graphene with single vacancy and adatom in order from top to bottom. The black lines in the band structures of defective graphene represent majority bands while red lines represent minority bands.

Table 1
The shortest vertical molecule-graphene distances (d) and binding energies (E_b) of C_6H_{12} on pristine graphene. We refer to Fig. 4 for the labeling of the sites. Distances are in Å and energies in meV.

Parallel			Perpendicular		
Site	d	E_b	Site	d	E_b
A	2.59	286	a	2.58	189
B	2.56	288	b	2.43	210
BC	2.46	311	c	2.58	187
C	2.47	321	d	2.57	206
Ar	2.56	299	ar	2.56	199
Br	2.54	301	br	2.56	191
BCr	2.46	299	cr	2.38	188

bond of graphene, as also noted previously [45]. In the GGA ground state, the C adatom is covalently bonded to graphene through two equivalent C—C bonds with bond lengths of 1.51 Å. The adatom is spin-polarized with a magnetic moment of 0.43 μ_B in agreement with previous work [50].

3.2. C_6H_{12}, $C_6H^*_{11}$ and C_6H_{10} adsorption on pristine graphene

To identify the preferred adsorption geometry of C_6H_{12}, 14 representative initial configurations were generated and subjected to tight structural optimization at the vdW-DF2^{C09x} level. Configurations in which the mean-plane of the molecule is either parallel or perpendicular to the graphene layer were considered. All initial configurations are shown in Fig. 4 along with labels where the letter r in a site label indicates a configuration in which the molecule is rotated by 30° with respect to the configuration without the letter r. Upon structural optimization, molecules were seen to deviate only slightly from their starting orientations. Calculated binding energies and C_6H_{12}-graphene vertical distances for a coverage of $\Theta = 1/36$ ML are reported in Table 1.

The most stable geometry for C_6H_{12} adsorption on graphene is configuration C, which corresponds to a parallel orientation of the graphene and molecular mean planes where the axial H atoms of C_6H_{12} facing the graphene layer are located directly above the centers of the empty hexagonal sites of the honeycomb lattice. C_6H_{12} is located at a distance of 2.47 Å and the calculated adsorption energy is 321 meV. A standard GGA calculation yields a molecule–graphene distance of about 3.12 Å and a binding energy of only 43 meV, highlighting thus the importance of the inclusion of dispersive forces. For C_6H_{12} adsorption at site C, upon increasing the coverage from $\Theta = 1/36$ ML to $\Theta = 1/9$ ML, the adsorbate-graphene distance was observed to increase only very slightly from 2.47 Å to 2.49 Å, while the calculated adsorption energy decreased by only about 68 meV. This indicates that the lateral interaction energies between adsorbates, are too low to contribute significantly at different coverages. Therefore, we will focus on the 1/36 ML coverage in the following. Overall, the perpendicular adsorption configurations are destabilized with respect to the parallel orientations by energy differences in the range 78–124 meV as reported in Table 1. These energy differences can be accounted for by the greater portion of the molecular surface exposed to graphene in the case of parallel adsorption. The C_6H_{12} binding energy at the PBE-D2 level for configuration C is 379 meV in good agreement with the vdW-DF2^{C09x} value.

A similar surface scan of the graphene layer involving both parallel and perpendicular geometries was conducted in the case of the radical species, $C_6H^*_{11}$. In many of the configurations explored, geometry optimization resulted in the formation of a covalent bond between the unsaturated C atom of the radical and graphene. This preliminary survey suggests that the $C_6H^*_{11}$ radical is more likely to bind covalently to both pristine and defective graphene, and therefore only chemisorbed $C_6H^*_{11}$–graphene configurations will be discussed in the following.

Similarly to C_6H_{12}, C_6H_{10} only physisorbs on pristine graphene. To make a direct comparison possible, C_6H_{10} adsorption on pristine

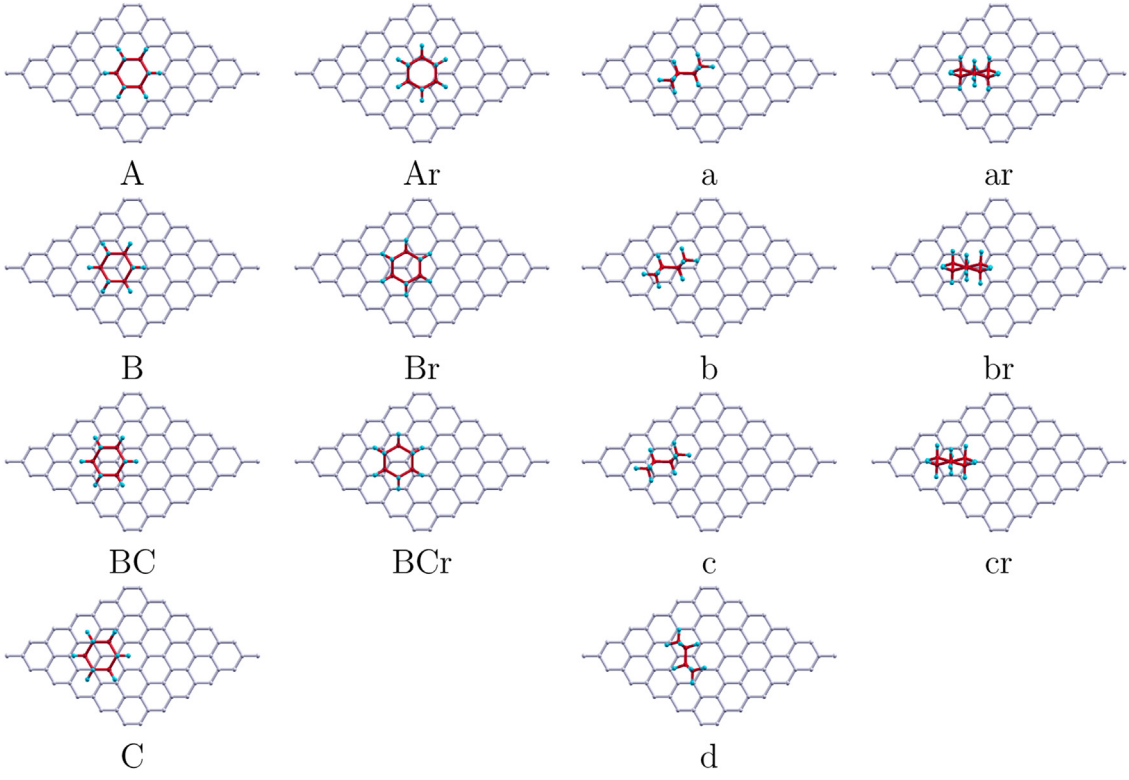

Fig. 4. Representative C_6H_{12} adsorption sites on graphene in a 6 × 6 simulation cell.

Table 2
The molecule–graphene distances (d) (defined as shortest vertical distance in the case of physisorption and bond length in the case of a covalent bond formation), binding energies (E_b), Bader charges ($|e|$) and magnetic moments (μ) of the adsorbates on pristine and defective graphene. Distances are in Å, energies are in eV and magnetic moments are in units of μ_B. Adsorption energies for physisorbed molecules where spin-polarization is important are calculated within PBE-D2. See text for details.

	Pristine				Single Vacancy				C adatom			
	d	E_b	q	μ	d	E_b	q	μ	d	E_b	q	μ
C_6H_{12}	2.47	0.32	0.001	0.00	2.34	0.36	-0.008	1.39	2.17	0.16	-0.01	0.47
$C_6H^*_{11}$	1.64	0.33	0.13	0.11	1.54	2.62	0.14	0.11	1.46	3.59	0.25	1.00
C_6H_{10}	2.38	0.39	0.002	0.00	2.35	0.47	0.001	1.41	1.48	3.43	0.19	0.00

graphene was considered at the on-top site (site C) as well. The calculated adsorption energy is 391 meV and the graphene-molecule distance is 2.38 Å as shown in Table 2 where the relevant parameters of all the adsorption geometries discussed in this paper are reported.

As a result of the weak interaction involved, adsorption of C_6H_{12} on pristine graphene does not affect the linear dispersion around the Fermi level (Fig. 5). The additional molecular states fall in the conduction and valence bands. Conversely, a flat band develops in the $C_6H^*_{11}$–graphene system as a consequence of chemisorption, coinciding with the Fermi level, and the degeneracy of the π and π^* bands is partially lifted. This state is localized to a large extent on the adsorbate, and the honeycomb C-atoms in close proximity to the sp^3-hybridized C atom of graphene. The $C_6H^*_{11}$/graphene system develops a slight magnetic moment of about 0.11 μ_B (Table 2). The charge density rearrangement upon adsorption is not confined only to the newly formed C-C bond between the adsorbate and the substrate (Fig. 5). In the case of cyclohexene, the noncovalent nature of the interaction with graphene does not perturb the linear dispersion around the Dirac point as seen in the band structure in Fig. 5. Moreover, a molecular band is visible at about 1.5 eV below the Fermi level.

The partial charges on the adsorbates are presented in Table 2. The charge transfer between the substrate and the molecule is

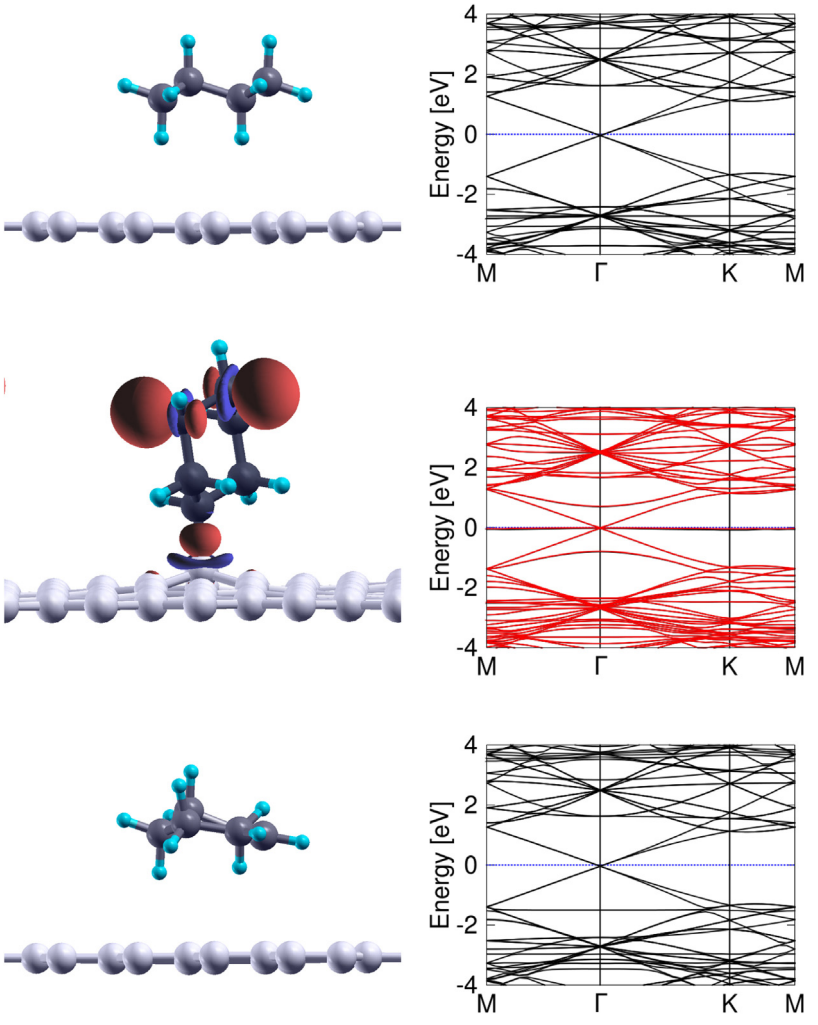

Fig. 5. Optimized geometries and band structures of representative C_6H_{12}, $C_6H^*_{11}$ and C_6H_{10} adsorption configurations on pristine graphene. The dark gray spheres represent the molecule C atoms, the light gray spheres represent the graphene C atoms and light blue spheres represent H atoms. Charge density difference plot is also shown in the middle panel for $C_6H^*_{11}$ at an isolvalue of 0.009 $|e|$/Bohr^3. Blue color represents electron deficient regions and red represents electron excess. For spin-polarized calculations, black lines represent majority bands while red lines represent minority bands. (For interpretation of the references to color in this figure legend, the reader is referred to the web version of this article.)

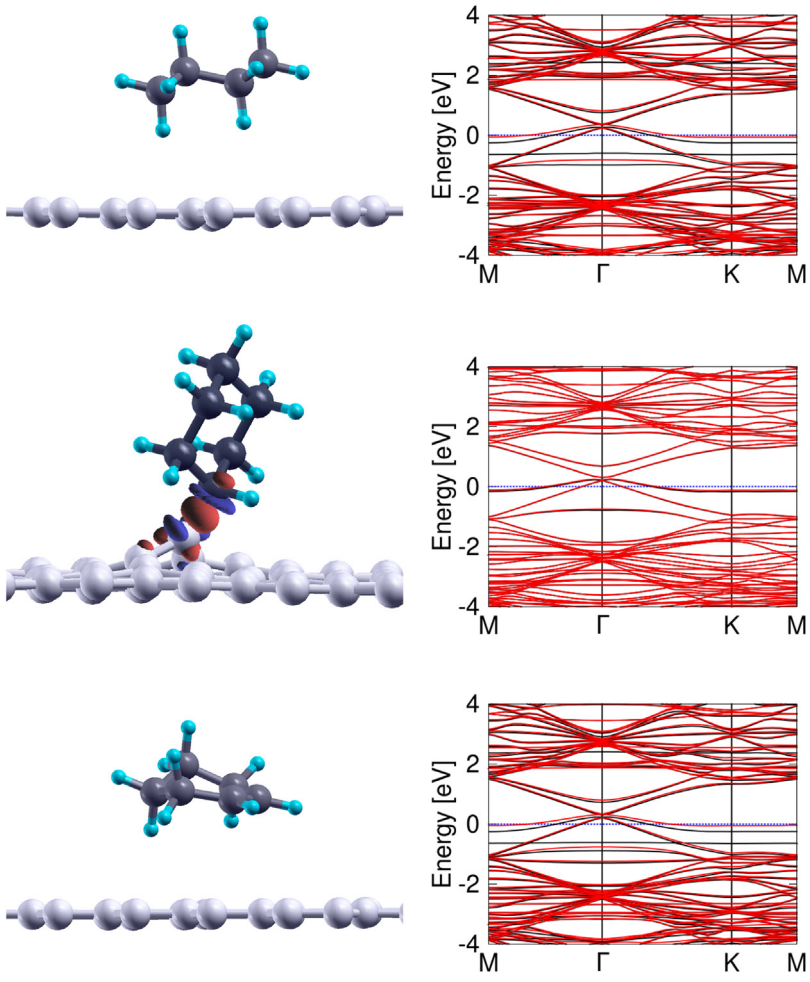

Fig. 6. Optimized geometries and band structures of representative C_6H_{12}, $C_6H_{11}^*$ and C_6H_{10} adsorption configurations on graphene with a single vacancy. The dark gray spheres represent the molecule C atoms, the light gray spheres represent the graphene C atoms and light blue spheres represent H atoms. Charge density difference plot is also shown in the middle panel for $C_6H_{11}^*$ at an isolvalue of 0.009 $|e|$/Bohr^3. Blue color represents electron deficient regions and red represents electron excess. For spin-polarized calculations, black lines represent majority bands while red lines represent minority bands. (For interpretation of the references to color in this figure legend, the reader is referred to the web version of this article.)

negligibly small for the physisorbed species (C_6H_{12} and C_6H_{10}) while $C_6H_{11}^*$ donates a charge of 0.13 $|e|$ to the graphene network.

3.3. Molecular adsorption on defective graphene

The interaction of C_6H_{12} both with the single vacancy (Fig. 6) and the adatom (Fig. 7) is noncovalent in nature. The binding energy of the C_6H_{12} was calculated for a geometry in which the center of the molecule is directly above the unsaturated C atom for the vacancy and the extra C for the adatom. This location was chosen to resemble configuration C for C_6H_{12} adsorption on pristine graphene. Handling of the spin degree of freedom requires additional care. Since the vacancy formation energy for spin-zero and spin-polarized states are very close (ΔE_{ads} = 0.19 eV) as noted earlier, both possibilities were explored. In the spin-unpolarized calculation, the vdW-DF2^{C09x} level of theory was used where the C_6H_{12} molecule was initially placed on flat graphene with the single vacancy. During geometric optimization the planarity of the graphene sheet was disturbed by the out-of-plane displacement of the unsaturated C atom by about 0.6 Å. The spin-polarized calculation, on the other hand, yields a planar geometry (Fig. 6), with a calculated magnetic moment of μ = 1.39 μ_B/cell and a molecule-substrate distance of about 2.34 Å. In spite of the sizable structural and electronic differences between the two configurations, the binding energies were found to be similar, 287 meV for the spin-unpolarized calculation and 358 meV for the spin-polarized calculation. In Fig. 6, we report the optimized geometry and band structure of the spin-polarized calculation. As a consequence of the weak binding, the effect of the adsorbate on the band structure is negligible, also supported by the lack of charge transfer between graphene and C_6H_{12} (Fig. 2 and Table 2). The molecular states do not contribute near the Fermi level and they all appear deeper into the valence band (between −2 and −16 eV) with very little contribution to the conduction band near 5 eV.

Similar spin-polarized and spin-restricted calculations were performed also for C_6H_{10} adsorption on the single vacancy at the on-top site described above for C_6H_{12}. The spin-unpolarized vdW-DF2^{C09x} calculation gave a binding energy of 396 meV while the binding energy for the spin-polarized calculation, carried out at the PBE-D2 level, was 473 meV (μ = 1.41 μ_B/cell). The PBE-D2 band structure displayed in Fig. 6 is very similar to the band structure of the isolated defective graphene around the Fermi level.

$C_6H_{11}^*$, on the other hand, makes a covalent C–C bond with the unsaturated C atom of the vacancy (Fig. 6) with a bond length of 1.54 Å. The resulting upward distortion induces strain on the surrounding bonds, increasing their length from 1.36 Å to 1.42 Å. Upon the formation of the covalent bond, the spin polarization is reduced to 0.11 μ_B, changing the band structure dramatically. The two spin-polarized bands, coming in just under the Fermi level at the Γ point

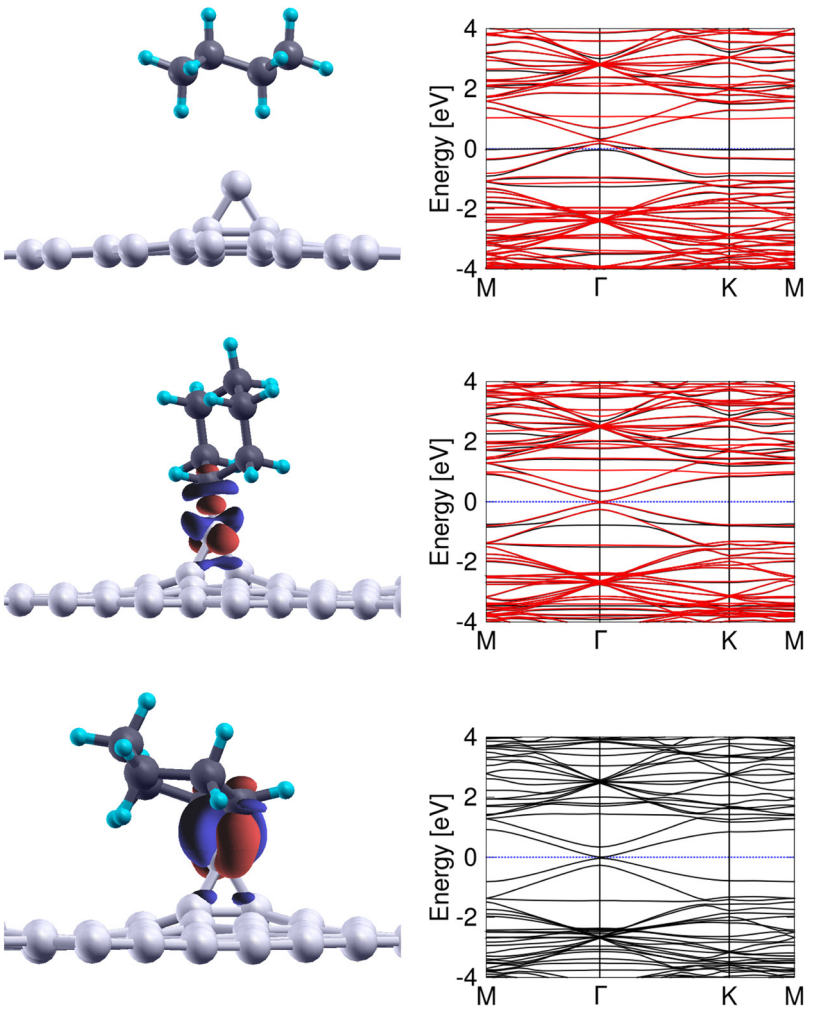

Fig. 7. Optimized geometries and band structures of representative C_6H_{12}, $C_6H^*_{11}$ and C_6H_{10} adsorption configurations on graphene with a C adatom. The dark gray spheres represent the molecule C atoms, the light gray spheres represent the graphene C atoms and light blue spheres represent H atoms. Charge density difference plot is also shown in the middle and lower panels for $C_6H^*_{11}$ and C_6H_{10} at an isolvalue of 0.009 $|e|$/Bohr^3. Blue color represents electron deficient regions and red represents electron excess. For spin-polarized calculations, black lines represent majority bands while red lines represent minority bands. (For interpretation of the references to color in this figure legend, the reader is referred to the web version of this article.)

collapse onto one another and the flat band around −0.5 eV disappears. In Fig. 6 we also report the charge density difference plot. However its analysis does not add new information besides the obvious signature of a C—C bond formation between the adsorbate and defective graphene. The computed GGA binding energy is 2.62 eV.

C_6H_{12} adsorption on the adatom (Fig. 7) is the weakest among all physisorbed configurations, with an adsorption energy of only 155 meV ($\mu = 0.47\mu_B$). The origin of this low adsorption energy is possibly the diminished contact area between the molecule and graphene plane in comparison to the other physisorbed molecules. The band structure is once again largely unaltered with respect to the isolated defective graphene. Both $C_6H^*_{11}$ and C_6H_{10}, on the other hand, bind covalently with the adatom. $C_6H^*_{11}$ adsorbs with a binding energy of 3.59 eV and the newly formed C—C bond has a length of 1.46 Å. The Fermi level is shifted upwards, while at the same time the flat majority spin band at the Fermi level disappears. The magnetic moment is 1.0 μ_B, supplied by the band around −0.5 eV. C_6H_{10} binds to the adatom through two C—C bonds each with a bond length of 1.48 Å and with a binding energy of 3.43 eV. For both $C_6H^*_{11}$ and C_6H_{10} the electron charge redistribution upon chemisorbtion on graphene is consistent with the formation of a C—C single bond. Once the adatom is fully saturated in this way, the system becomes spin unpolarized and the flat band at the Fermi level disappears. In addition, the Fermi level shifts upwards as in the case of C_6H_{12}.

Similarly to the case of adsorption on pristine graphene, physisorbed species do not experience any significant charge transfer upon adsorption on defective graphene (Table 2). For all chemisorbed species, the charge transfer is from the adsorbate to the graphene layer with values of 0.14 $|e|$, 0.25 $|e|$ and 0.19 $|e|$ respectively for $C_6H^*_{11}$ on vacancy, $C_6H^*_{11}$ on adatom and C_6H_{10} on adatom.

4. Conclusion

In this work, the adsorption of cyclohexane (C_6H_{12}) and its dehydrogenated derivatives, the cyclohexyl radical ($C_6H^*_{11}$) and cyclohexene (C_6H_{10}) on pristine and defective (C vacancy and C adatom) graphene was explored at the GGA, PBE-D2, and vdW-DF2^{C09x} level of theory. The selection of molecules offers the possibility of exploring a range of covalent and non-covalent interactions with pristine and defective graphene. A solid understanding of both adsorption modes are fundamental to industrial applications.

In all cases explored, C_6H_{12} binds via weak attractive forces and causes only small changes to the band structure of graphene.

C_6H_{10}, with a single double bond between two neighboring atoms, is more conducive to participating in sp^3 hybrids and as a result makes a covalent bond with the adatom. However, it is still found to physisorb onto pristine graphene and graphene with a single vacancy. In contrast to C_6H_{12} and C_6H_{10}, $C_6H_{11}^*$ binds with pristine and defective graphene through the formation of a strong covalent bond. Physisorbed geometries do not disturb the band structures in any significant manner and as a result preserve the original spin-polarization for the vacancy and the adatom. All covalently bonded geometries result in little to no spin polarization with the exception of $C_6H_{11}^*$ on the adatom. The varied characteristics of interaction between the molecules studied in this work can be utilized for applications as dissimilar as intercalation of graphene and catalysis. In particular, the relatively under-explored field of molecular functionalization of defective graphene promises a rich variety of bonding configurations, providing a convenient handle for applications involving band structure modification.

Graphene has been proposed as an absorbent for organic molecules for catalytic and environmental applications [51]. This could especially be important for C_6H_{12} and C_6H_{10}, which are abundant byproducts of petrochemical industries and have both been identified as hazardous to human health [52,53]. The physisorption energies that we report in this work for both species are comparable to adsorption of benzene on pure or processed graphene [54] and consequently their adsorption on graphene can be considered a functioning capture and elimination mechanism. Furthermore, interaction of C_6H_{12} with carbon-based materials has taken center-stage in other important applications including exfoliation of graphene in solution [55], metal-free selective oxidation of saturated hydrocarbons [27,31] and the characterization of multi-walled carbon nanotubes using hydrocarbons [28]. As regards geometries that exhibit covalent bonding, we report a charge transfer from the molecule to the graphene network. This points towards potential use in device technology where controlled doping in graphene is important.

Acknowledgements

We gratefully acknowledge the computational resources provided by ULAKBIM-GRID National Computing Center of Turkey.

References

[1] K.S. Novoselov, D. Jiang, F. Schedin, T.J. Booth, V.V. Khotkevich, S.V. Morozov, A.K. Geim, Two-dimensional atomic crystals, Proc. Natl. Acad. Sci. U. S. A. 102 (2005) 10451–10453.
[2] L. Brey, H. Fertig, Electronic states of graphene nanoribbons studied with the Dirac equation, Phys. Rev. B 73 (2006) 235411.
[3] A. Shytov, M. Rudner, N. Gu, M. Katsnelson, L. Levitov, Atomic collapse, Lorentz boosts, Klein scattering, and other quantum-relativistic phenomena in graphene, Solid State Commun. 149 (2009) 1087–1093.
[4] F. Xia, D.B. Farmer, Y.-M. Lin, P. Avouris, Graphene field-effect transistors with high on/off current ratio and large transport band gap at room temperature, Nano Lett. 10 (2010) 715–718.
[5] S.H. Jin, D.H. Kim, G.H. Jun, S.H. Hong, S. Jeon, Tuning the photoluminescence of graphene quantum dots through the charge transfer effect of functional groups, ACS Nano 7 (2013) 1239–1245.
[6] R.W. Havener, Y. Liang, L. Brown, L. Yang, J. Park, Van Hove singularities and excitonic effects in the optical conductivity of twisted bilayer graphene, Nano Lett. 14 (2014) 3353–3357.
[7] Y. Qiao, X.-S. Wu, C.-X. Ma, H. He, C.M. Li, A hierarchical porous graphene/nickel anode that simultaneously boosts the bio- and electro-catalysis for high-performance microbial fuel cells, RSC Adv. 4 (2014) 21788–21793.
[8] K. Bolotin, K. Sikes, Z. Jiang, M. Klima, G. Fudenberg, J. Hone, P. Kim, H. Stormer, Ultrahigh electron mobility in suspended graphene, Solid State Commun. 146 (2008) 351–355.
[9] A.A. Balandin, S. Ghosh, W. Bao, I. Calizo, D. Teweldebrhan, F. Miao, C.N. Lau, Superior thermal conductivity of single-layer graphene, Nano Lett. 8 (2008) 902–907.
[10] C. Lee, X. Wei, J.W. Kysar, J. Hone, Measurement of the elastic properties and intrinsic strength of monolayer graphene, Science 321 (2008) 358–385.
[11] F. Schedin, A.K. Geim, S.V. Morozov, E.W. Hill, P. Blake, M.I. Katsnelson, K.S. Novoselov, Detection of individual gas molecules adsorbed on graphene, Nat. Mater. 6 (2007) 652–655.
[12] V. Georgakilas, M. Otyepka, A.B. Bourlinos, V. Chandra, N. Kim, K.C. Kemp, P. Hobza, R. Zboril, K.S. Kim, Functionalization of graphene: covalent and non-covalent approaches, derivatives and applications, Chem. Rev. 112 (2012) 6156–6214.
[13] D.W. Boukhvalov, M.I. Katsnelson, Chemical functionalization of graphene, J. Phys.: Condens. Matter 21 (2009) 344205.
[14] T. Kuila, S. Bose, A. Kumar, P. Khanra, Chemical functionalization of graphene and its applications, Prog. Mater. Sci. 57 (2012) 1061–1105.
[15] H.Y. Mao, Y.H. Lu, J.D. Lin, S. Zhong, A.T.S. Wee, W. Chen, Manipulating the electronic and chemical properties of graphene via molecular functionalization, Prog. Surf. Sci. 88 (2013) 132–159.
[16] R. Balog, M. Andersen, B. Jrgensen, Z. Sljivancanin, B. Hammer, A. Baraldi, R. Larciprete, P. Hofmann, L. Hornekr, S. Lizzit, Controlling hydrogenation of graphene on Ir(1 1 1), ACS Nano 7 (2013) 3823–3832.
[17] F. Karlický, M. Otyepka, Band gaps and optical spectra of chlorographene, fluorographene and graphane from G_0W_0, GW_0 and GW calculations on top of PBE and HSE06 orbitals, J. Chem. Theory Comput. 9 (2013) 4155–4164.
[18] J.A. Mann, W.R. Dichtel, Noncovalent functionalization of graphene by molecular and polymeric adsorbates, J. Phys. Chem. Lett. 4 (2013) 2649–2657.
[19] E. Chigo Anota, A. Torres Soto, G. Cocoletzi, Studies of graphene–chitosan interactions and analysis of the bioadsorption of glucose and cholesterol, Appl. Nanosci. 4 (2014) 911–918.
[20] C. Coletti, C. Riedl, D.S. Lee, B. Krauss, L. Patthey, K. von Klitzing, J.H. Smet, U. Starke, Charge neutrality and band-gap tuning of epitaxial graphene on SiC by molecular doping, Phys. Rev. B 81 (2010) 235401.
[21] Y.-H. Zhang, Y.-B. Chen, K.-G. Zhou, C.-H. Liu, J. Zeng, H.-L. Zhang, Y. Peng, Improving gas sensing properties of graphene by introducing dopants and defects: a first-principles study, Nanotechnology 20 (2009) 185504.
[22] D.W. Boukhvalov, M.I. Katsnelson, Chemical functionalization of graphene with defects, Nano Lett. 8 (2008) 4373–4379.
[23] O. Cretu, A.V. Krasheninnikov, J.A. Rodríguez-Manzo, L. Sun, R.M. Nieminen, F. Banhart, Migration and localization of metal atoms on strained graphene, Phys. Rev. Lett. 105 (2010) 196102.
[24] X. Wang, S.M. Tabakman, H. Dai, Atomic layer deposition of metal oxides on pristine and functionalized graphene, J. Am. Chem. Soc. 130 (2008) 8152–8153.
[25] F. Banhart, J. Kotakoski, A.V. Krasheninnikov, Structural defects in graphene, ACS Nano 5 (2011) 26–41.
[26] G. L, R. Zhao, G. Qian, Y. Qi, X. Wang, J. Suo, A highly efficient catalyst Au/MCM-41 for selective oxidation cyclohexane using oxygen, Catal. Lett. 97 (2004) 115–118.
[27] H. Yu, F. Peng, J. Tan, X. Hu, H. Wang, J. Yang, W. Zheng, Selective catalysis of the aerobic oxidation of cyclohexane in the liquid phase by carbon nanotubes, Angew. Chem. Int. Ed. 50 (2011) 3978–3982.
[28] E.W. Bittner, M.R. Smith, B.C. Bockrath, Characterization of the surfaces of single-walled carbon nanotubes using alcohols and hydrocarbons: a pulse adsorption technique, Carbon 41 (2003) 1231–1239.
[29] E. Díaz, S. Ordóñez, A. Vega, Adsorption of volatile organic compounds onto carbon nanotubes, carbon nanofibers, and high-surface-area graphites, J. Colloid Interface Sci. 305 (2007) 7–16.
[30] J. Zhao, J.P. Lu, J. Han, C.-K. Yang, Noncovalent functionalization of carbon nanotubes by aromatic organic molecules, Appl. Phys. Lett. 82 (2003) 3746–3748.
[31] X. Yang, H. Wang, J. Li, W. Zheng, R. Xiang, Z. Tang, H. Yu, F. Peng, Mechanistic insight into the catalytic oxidation of cyclohexane over carbon nanotubes: kinetic and in situ spectroscopic evidence, Chem. Eur. J. 19 (2013) 9818–9824.
[32] P. Giannozzi, łatin, et al., QUANTUM ESPRESSO: a modular and open-source software project for quantum simulations of materials, J. Phys.: Condens. Matter 21 (2009) 395502.
[33] D. Vanderbilt, Soft self-consistent pseudopotentials in a generalized eigenvalue formalism, Phys. Rev. B 41 (1990) 7892–7895.
[34] J.P. Perdew, K. Burke, M. Ernzerhof, Generalized gradient approximation made simple, Phys. Rev. Lett. 77 (1996) 3865–3868.
[35] G. Román-Pérez, J.M. Soler, Efficient implementation of a van der Waals density functional: application to double-wall carbon nanotubes, Phys. Rev. Lett. 103 (2009) 096102.
[36] K. Lee, E.D. Murray, L. Kong, B.I. Lundqvist, D.C. Langreth, Higher-accuracy van der Waals density functional, Phys. Rev. B 82 (2010) 081101.
[37] V.R. Cooper, Van der Waals density functional: an appropriate exchange functional, Phys. Rev. B 81 (2010), 161104(R).
[38] S. Grimme, Semiempirical GGA-type density functional constructed with a long-range dispersion correction, J. Comput. Chem. 27 (2006) 1787–1799.
[39] N. Marzari, D. Vanderbilt, A. De Vita, M.C. Payne, Thermal contraction and disordering of the Al(1 1 0) surface, Phys. Rev. Lett. 82 (1999) 3296–3299.
[40] W. Gao, P. Xiao, G. Henkelman, K.M. Liechti, R. Huang, Interfacial adhesion between graphene and silicon dioxide by density functional theory with van der Waals corrections, J. Phys. D: Appl. Phys. 47 (2014) 255301.
[41] A. Kokalj, XCrySDen a new program for displaying crystalline structures and electron densities, J. Mol. Graph. Model. 17 (1999) 176–179.
[42] NIST Computational Chemistry Comparison and Benchmark Database, NIST Standard Reference Database Number 101, 2013. http://cccbdb.nist.gov/, Release 16a.
[43] R. Kahn, R. Fourme, D. André, M. Renaud, Crystal structure of cyclohexane I and II, Acta Crystallogr. Sect. B Struct. Crystallogr. Crystal Chem. B29 (1973) 131–138.

[44] X.Q. Dai, J.H. Zhao, M.H. Xie, Y.N. Tang, Y.H. Li, B. Zhao, First-principle study of magnetism induced by vacancies in graphene, Eur. Phys. J. B 80 (2011) 343–349.
[45] L. Li, S. Reich, J. Robertson, Defect energies of graphite: density-functional calculations, Phys. Rev. B 72 (2005) 184109.
[46] G. Henkelman, A. Arnaldsson, H. Jónsson, A fast and robust algorithm for Bader decomposition of charge density, Comput. Mater. Sci. 36 (2006) 354–360.
[47] W.S. Paz, W.L. Scopel, J.C. Freitas, On the connection between structural distortion and magnetism in graphene with a single vacancy, Solid State Commun. 175-176 (2013) 71–75.
[48] B.R.K. Nanda, M. Sherafati, Z.S. Popovi, S. Satpathy, Electronic structure of the substitutional vacancy in graphene: density-functional and Green's function studies, New J. Phys. 14 (2012) 083004.
[49] B. Wang, S.T. Pantelides, Magnetic moment of a single vacancy in graphene and semiconducting nanoribbons, Phys. Rev. B 86 (2012) 165438.
[50] P.O. Lehtinen, A.S. Foster, A. Ayuela, A. Krasheninnikov, K. Nordlund, R.M. Nieminen, Magnetic properties and diffusion of adatoms on a graphene sheet, Phys. Rev. Lett. 91 (2003) 017202.
[51] M. Kragulj, J. Trickovic, B. Dalmacija, A. Kukovecz, Z. Konya, J. Molnar, S. Roncevic, Molecular interactions between organic compounds and functionally modified multiwalled carbon nanotubes, Chem. Eng. J. 225 (2013) 144–152.
[52] V. Cocheo, M.L. Bellomo, G.G. Bombi, Rubber manufacture: sampling and identification of volatile pollutants, Am. Ind. Hyg. Assoc. J. 44 (1983) 521–527.
[53] Office Of Pollution Prevention And Toxics, U.S. Environmental Protection Agency, 1994. www.epa.gov/chemfact
[54] O.V. Ershova, T.C. Lillestolen, E. Bichoutskaia, Study of polycyclic aromatic hydrocarbons adsorbed on graphene using density functional theory with empirical dispersion correction, Phys. Chem. Chem. Phys. 12 (2010) 6483–6491.
[55] Z. Tang, J. Zhuang, X. Wang, Exfoliation of graphene from graphite and their self-assembly at the oil–water interface, Langmuir 26 (2010) 9045–9049.